A multifunctional 3.5 V iron-based phosphate cathode for rechargeable batteries

B. L. ELLIS, W. R. M. MAKAHNOUK, Y. MAKIMURA, K. TOGHILL AND L. F. NAZAR*

Department of Chemistry, University of Waterloo, 200 University Ave. W., Waterloo, Ontario, N2L 3G1, Canada

*e-mail: lfnazar@uwaterloo.ca

Published online: 9 September 2007; doi:10.1038/nmat2007

In the search for new positive-electrode materials for lithium-ion batteries, recent research has focused on nanostructured lithium transition-metal phosphates that exhibit desirable properties such as high energy storage capacity combined with electrochemical stability[1,2]. Only one member of this class—the olivine $LiFePO_4$ (ref. 3)—has risen to prominence so far, owing to its other characteristics, which include low cost, low environmental impact and safety. These are critical for large-capacity systems such as plug-in hybrid electric vehicles. Nonetheless, olivine has some inherent shortcomings, including one-dimensional lithium-ion transport and a two-phase redox reaction that together limit the mobility of the phase boundary[4–7]. Thus, nanocrystallites are key to enable fast rate behaviour[8,9]. It has also been suggested that the long-term economic viability of large-scale Li-ion energy storage systems could be ultimately limited by global lithium reserves, although this remains speculative at present. (Current proven world reserves should be sufficient for the hybrid electric vehicle market, although plug-in hybrid electric vehicle and electric vehicle expansion would put considerable strain on resources and hence cost effectiveness.) Here, we report on a sodium/lithium iron phosphate, A_2FePO_4F (A = Na, Li), that could serve as a cathode in either Li-ion or Na-ion cells. Furthermore, it possesses facile two-dimensional pathways for Li^+ transport, and the structural changes on reduction–oxidation are minimal. This results in a volume change of only 3.7% that—unlike the olivine—contributes to the absence of distinct two-phase behaviour during redox, and a reversible capacity that is 85% of theoretical.

The discovery of new materials such as phosphates and silicates that exhibit good electrochemical properties at beneficial redox potentials is of timely significance, as they present considerable safety advantages over the more commonly used metal oxides. Lithium metal fluorophosphates have also recently emerged as promising candidates. Their analogues in the mineral world are hydroxyfluorophosphates, including calcium hydroxyfluoroapatite (the element of teeth) and tavorite [$LiFePO_4(OH,F)$], where F^- can partially replace an OH^- group. Complete substitution of F^- is necessary for electrochemical properties because the hydroxy group undergoes irreversible redox reactivity. Moreover, replacement of $[PO_4]^{3-}$ with $[PO_4F]^{4-}$ allows for a new family of host lattice structures and compositions, as it alters the charge balance, and the dimensionality of the structure vis-à-vis the corresponding phosphate[10]. However, only a few lithium transition-metal fluorophosphates have been described so far[10–13].

In the quest for other new materials, a sodium fluorophosphate, $Na_3V_2(PO_4)_2F_3$, was recently shown to be an excellent candidate for 'hybrid-ion' cells in concert with a carbon anode[14]. In the initial oxidation, sodium ions are extracted from the fluorophosphate while concurrent lithium-ion intercalation occurs at the graphite counter electrode. During subsequent cell cycling, the cathode reaction is described as a mixed Li/Na insertion mechanism. The important point is that the carbon anode is completely electrochemically stable in the presence of Na^+ in the electrolyte phase. The more significant aspect is that alternatives to Li-ion storage cells might be necessary in the future if the hybrid electric vehicle/plug-in hybrid electric vehicle/electric vehicle and overall energy storage market grows as anticipated. Recent findings estimate that the terrestrial reserves of lithium could be rapidly depleted, considering that large-scale cells require 100–500 times the amount of lithium as portable devices. The issue is not insufficient lithium on a global scale, but what fraction can be used and still be economically effective. A possible option is Na-ion cells. These could include Zebra cells (Na–$NiCl_2$) that function with liquid sodium by a displacement reaction at ~300 °C (ref. 15), or insertion materials that operate at 25 °C and offer higher energy density, akin to Li-ion cells. In the latter context, negative electrodes based on hard carbons have been shown to exhibit excellent properties for Na-ion insertion, with up to 350 mAh g^{-1} capacity[16,17]. Coupled to a suitable Na-ion insertion cathode, such a system would offer the necessary safety characteristics at much lower cost and be able to use electrolytes of lower decomposition voltage. However, the obvious cathode material, $NaFePO_4$, is not suitable. The 'closed' maricite framework results in entrapment of Na^+ and no reversible redox behaviour.

Inspired by these considerations, we sought to synthesize an environmentally friendly iron-based alkali fluorophosphate that operates on the $Fe^{2+} \rightarrow Fe^{3+}$ couple, which possesses facile pathways for alkali-ion diffusion, and which, like $LiFePO_4$, can be prepared in its reduced form to allow it to be used directly as a positive electrode. The structure of the new material, Na_2FePO_4F, that we prepared as a single crystal is shown in Fig. 1a. It crystallizes in the *Pbcn* orthrorhombic space group, isostructural with both Na_2FePO_4OH (ref. 18) and $Na_2Co(PO_4)F$ (ref. 19). Like the latter, its framework exhibits unusual features. Bioctahedral $Fe_2O_7F_2$ units comprising face-sharing FeO_4F_2 octahedra are connected via bridging F atoms to form chains, and are joined by PO_4 tetrahedra

© 2007 Nature Publishing Group

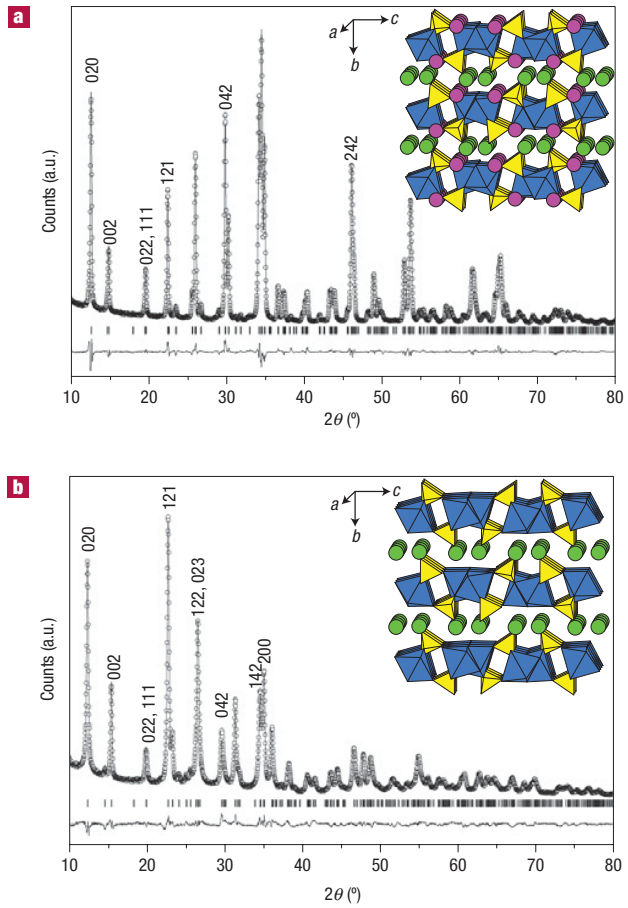

Figure 1 XRD patterns and structures of the pristine (Na_2FePO_4F) and oxidized material ($NaFePO_4F$). a, Structure of Na_2FePO_4F taken from single-crystal data shown along the [100] direction, together with the XRD pattern and Rietveld analysis of a single-phase microcrystalline powder of the same material; lattice parameters in *Pbcn* are $a = 5.2200(2)$ Å, $b = 13.8540(6)$ Å, $c = 11.7792(5)$ Å. Iron octahedra are shown in blue, and the phosphate tetrahedra in yellow; the two alkali sites are distinguished as Na (1) in green and Na (2) in pink. **b**, Structure of $NaFePO_4F$ derived from the Rietveld analysis as shown; lattice parameters in *Pbcn* are $a = 5.1047(9)$ Å, $b = 14.1326(2)$ Å, $c = 11.3655(1)$ Å. The loss of the Na (2) from the structure on oxidation was immediately evident when the occupancy of the Na (1) and (2) sites was allowed to vary.

to form $[FePO_4F]$ infinite layers. The two Na cations located in the interlayer space possess facile two-dimensional migration pathways and more limited transport in the third dimension. The structure is quite different from that of the analogous Na_2MnPO_4F (ref. 20) and Li_2NiPO_4F (ref. 11) compositions, which adopt tunnel rather than layered frameworks, and is also different from other layered fluorophosphates, such as $Na_5Fe(PO_4)_2F_2$ (ref. 21), or $Na_3M_2(PO_4)_2F_3$ (M = Cr, Al, V, Fe)[22]. Detailed aspects will be presented elsewhere. To examine the electrochemical properties of Na_2FePO_4F, we also prepared it as a nanostructured polycrystalline phase by both solid-state synthesis and a novel sol–gel route that incorporates 1–3% carbon on the surface of the material. Rietveld analysis of the X-ray diffraction (XRD) pattern confirmed the existence of a pure single phase (Fig. 1a), with lattice parameters the same as those obtained from single-crystal analysis. The scanning electron microscopy (SEM) images of the sol–gel material (Fig. 2a) reveal a uniform crystallite size distribution centred at about 200 nm. The carbon coating, estimated to be about 2–4 nm thick, is visible in the transmission electron microscope (TEM) image (Fig. 2b) and by elemental line-scan analysis (Fig. 2c). The sharp drop-off in Fe and P intensity demarcates the edge of the crystallite, just beyond which a sharp spike in carbon intensity above the background is evident. Nonetheless, the carbon is amorphous owing to the low processing temperature and the nature of the carbon source[23]. The conductivity of the coated material was estimated to be only 1.4×10^{-6} S cm^{-1} by two-probe d.c. measurements on pressed pellets, a factor of 1,000 less than seen for typical commercial $LiFePO_4$ electrode materials. Efforts are underway to increase this.

Electrodes prepared from this material were examined in coin-type cells, using lithium metal as a counter electrode. The cells were cycled at a rate corresponding to fully charging the theoretical capacity of the material in 10 h (C/10), using a typical active material loading in the range of 6–8 mg cm^{-2}. The voltage–discharge curve shown in Fig. 4 reveals a profile quite unlike that of the flat plateau of the iron olivine that is characteristic of the essentially two-phase reaction $LiFePO_4 \leftrightarrow FePO_4$. The sloping curve on oxidation for Na_2FePO_4F suggests the presence of a solid solution up to the composition $NaFePO_4F$ that corresponds to the limit of sodium extraction within this voltage window. After two cycles the profile transforms, and both the oxidation and reduction processes now suggest the presence of two sloping regimes that are present even under close-to-equilibrium conditions. (Close-to-equilibrium conditions are defined as C/50 or a galvanostatic intermittent titration.) These span either side of an $A_{1.5}FePO_4F$ phase that has an apparent solid-solution range, given the pronounced gradient in the voltage profile centred at that composition. This is in contrast with the very well-defined voltage jump that is a signature of formation of a stoichiometric single phase, as seen in $Li_{3-x}V_2(PO_4)_3$ (ref. 24). Mixed Li/Na (de)insertion predominantly favours Li after the first anodic sweep as cycling progresses, owing to the vast excess of Li^+ in the cell. Such a process will further add complexity to the voltage profile. Ion switching was confirmed by energy-dispersive X-ray spectroscopy (EDX) analysis of the recovered cathode material, which showed that the Na/Fe (or Na/P) ratio dropped immediately from 2:1 to 1:1 after the first cycle (see Supplementary Information, Fig. SA). These ratios continued to decrease, albeit more slowly, to approach a value of 0.5:1 after 15 cycles. Most significant is that ~80% of the theoretical capacity (135 mAh g^{-1}) is attainable on the first oxidation cycle. This reversible capacity is well sustained on cycling (Fig. 4, inset). Thus, the presence of sodium is not a deterrent, aside from incurring a small mass deficit. The advantage is that sodium iron fluorophosphate can be prepared at much lower cost than any lithium analogue, and used directly as a cathode with a lithium-salt electrolyte. In conjunction with a suitable Na-salt electrolyte and a hard-carbon anode[16], it comprises a Na-ion cell.

We note that the average charge potential of 3.6 V on cycling is similar to that of $LiFePO_4$ (3.55 V). Interestingly, the open-circuit voltage (OCV) is lower than that of the olivine (3.0 V versus 3.45 V) and higher than that of the $Fe^{3+/2+}$ couple in $Li_3Fe(PO_4)_3$ (2.8 V) (ref. 25). This is in part due to the initial presence of Na^+ in the lattice, which will slightly lower the redox potential. Moreover, framework connectivity determines the OCV of any given redox couple in these phosphates to a large extent. Thus, the all-corner-shared lattice of the metal and phosphorus polyhedra in $Li_3Fe(PO_4)_3$ leads to less repulsion between M^{n+} and P^{5+} and a lower redox potential—versus the edge-shared environment in the olivine that increases the OCV. The intermediate OCV of Na_2FePO_4F reflects its adaptation of both connectivity modes.

© 2007 Nature Publishing Group

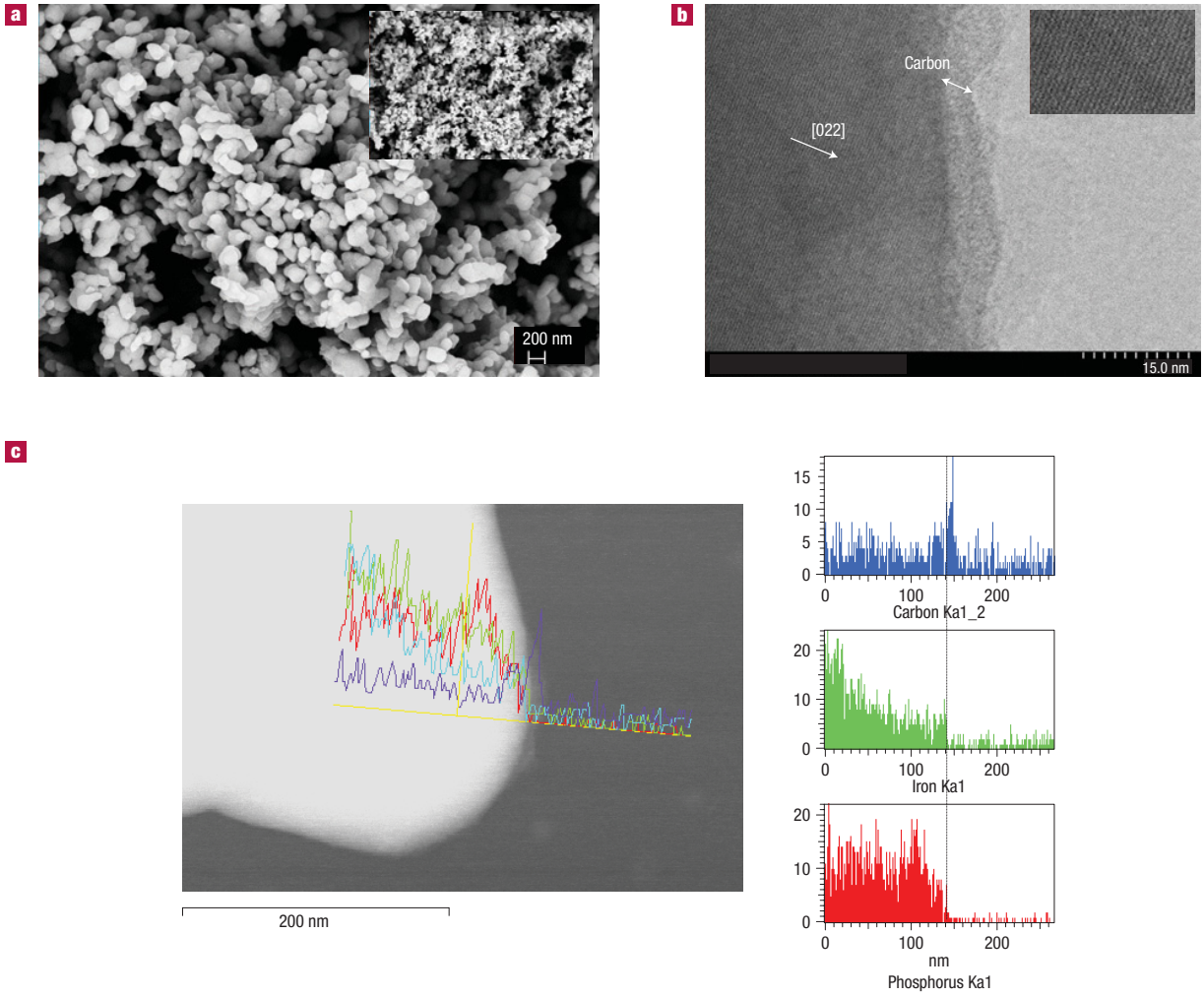

Figure 2 Electron microscopy analysis of Na_2FePO_4F. a, SEM of single-phase microcrystalline Na_2FePO_4F at ×20,000 magnification; inset at ×10,000 magnification illustrates good particle size homogeneity. **b**, TEM of a crystallite showing the lattice planes and a ~3 nm carbon coating on the surface. **c**, Electron energy-loss spectroscopy line-scan of a crystallite. The intensity of the elements Fe, P, O, Na and C are shown on the scan itself with respect to the particle, and expanded on the right for Fe, P and C.

The ease of the reversible redox process suggested to us that the structural changes on oxidation–reduction are minimal. To clarify this, we carried out chemical oxidation of $Na_2Fe^{II}PO_4F$ to form the single-phase $NaFe^{III}PO_4F$. The Na/Fe ratio of 1:1 in this material was verified by SEM–EDX analysis, which showed there is little change to the crystallite morphology vis-à-vis the parent phase. Rietveld analysis was carried out following an initial full-pattern match that identified that the space group of the parent phase was maintained. The fractional coordinates and thermal parameters of the atoms in the starting phase ($Na_2Fe^{II}PO_4F$) were refined along with the occupancy of the two sodium sites to give excellent agreement factors. The resulting structure derived from the Rietveld analysis is shown in Fig. 1b. The initial framework is maintained virtually unchanged on oxidation, with only a 3.7% volume contraction. The value is about half that sustained by the olivine $LiFePO_4 \leftrightarrow FePO_4$ couple (6.7%), and thus (de)intercalation in this framework is a lower-strain process. Complete loss of Na (2) from the structure occurs on oxidation—rather than loss of Na (1) or partial loss of both sodium cations. This may be explained by the slightly greater repulsion that is experienced by the former when ionic (Fe^{2+}–Na^{+}) interactions are considered. Furthermore, $Na_{1.5}FePO_4F$ is also a single phase with lattice parameters intermediate between the two end members, as summarized in Table 1 and shown in Fig. 3 (and see Supplementary Information, Fig. SB). Vegard's law is not precisely obeyed, as extraction of half of the alkali results in a very slight change in symmetry to a monoclinic unit cell ($\beta = 91.22°$; Table 1). Thus, transition between these two closely related phases results in the 'solid-solution-like' electrochemical behaviour over the redox range that is spanned by $Na_{2-x}FePO_4F$ ($x = 0 \rightarrow 1$).

Ion exchange of the sodium cations for lithium within the lattice was accomplished by refluxing Na_2FePO_4F in a solution of LiBr. One Na^{+} was readily displaced using mild exchange conditions (50 °C, 5 h) to produce the composition $LiNaFePO_4F$. EDX and chemical analysis both confirmed a 1:0.97 ratio of Fe/Na. This mixed ion phase which exhibits lattice parameters (Table 1) consistent with replacement of one sodium ion was also prepared by reductive lithiation of the oxidized phase $NaFePO_4F$

© 2007 Nature Publishing Group

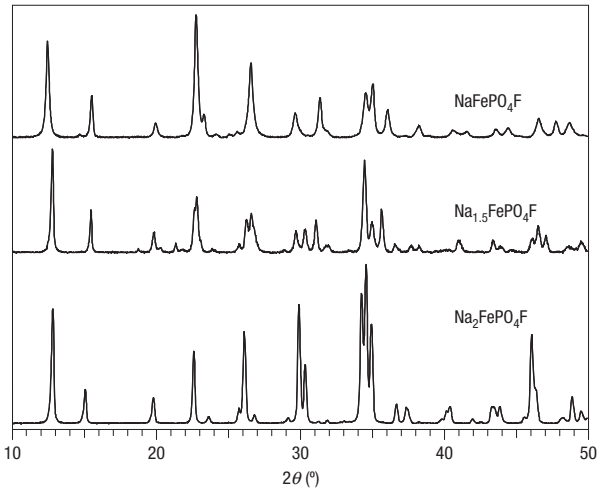

Figure 3 XRD patterns of Na_2FePO_4F, $Na_{1.5}FePO_4F$ and $NaFePO_4F$. They demonstrate 'quasi-solid-solution' behaviour that represents the transition between the two closely related phases.

Table 1 Lattice parameters and cell volume for $Na_xLi_yFePO_4F$.

	Space group	*a* (Å)	*b* (Å)	*c* (Å)	*β* (°)	Volume (Å^3)
* Na_2FePO_4F	*Pbcn*	5.2200(2)	13.8540(6)	11.7792(5)	90.00	851.85
† Na_2FePO_4F	*Pbcn*	5.24213	13.87231	11.79610	90.00	857.80
† $NaFePO_4F$	*Pbcn*	5.10479	14.13262	11.36551	90.00	820.00
† $Na_{1.5}FePO_4F$	*P2/c*	13.92967	5.20098	11.51471	91.22	834.03
‡ $NaLiFePO_4F$	*Pbcn*	5.07500	13.66000	11.13500	90.00	771.92
‡ Li_2FePO_4F	*Pbcn*	5.05500	13.56100	11.05200	90.00	757.62

* Single-crystal data.

† Values from Rietveld refinement of powder XRD data.

‡ Values from indexing powder XRD data. The slightly broadened features in the patterns prevented a satisfactory Rietveld refinement from converging.

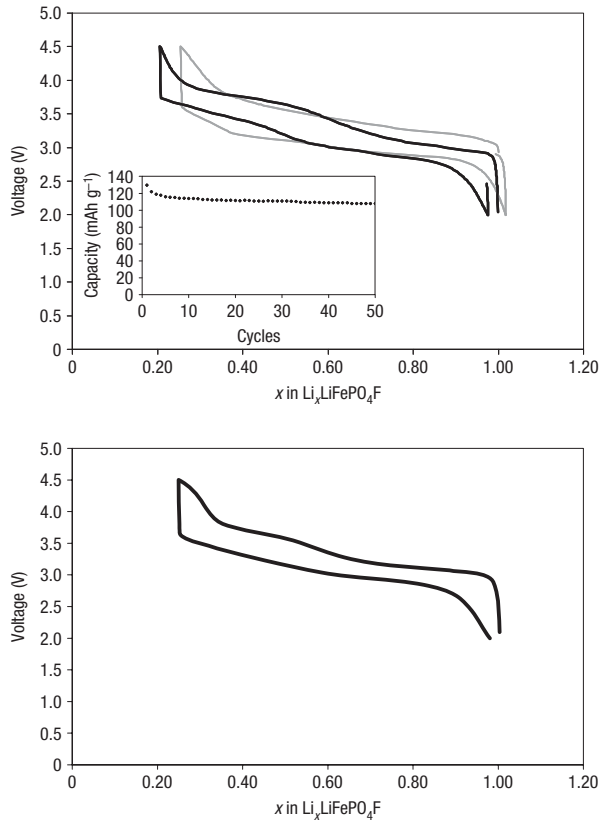

Figure 4 Electrochemical studies of A_2FePO_4F. a, Voltage charge–discharge curve of Na_2FePO_4F at C/10. Cycle 1 is shown in grey and cycle 2 in black. **b**, Voltage charge–discharge curve of Li_2FePO_4F obtained via ion exchange.

using LiI. Both Na (1) and (2) were displaced on more rigorous ion-exchange treatment. The latter phase has a Na:Fe content of about 0.20:1.0, and lattice parameters consistent with the formation of a highly lithiated composition (Table 1). We designate this material 'Li_2FePO_4F' for brevity. Its voltage charge–discharge profile shown in Fig. 4b reveals a shape very similar to that of Na_2FePO_4F after five cycles, and the same reversible capacity of ~80%. This further proves that Li preferentially replaces Na in the lattice on electrochemical cycling as described above. Structural and electrochemical studies to unravel the complexity of the ion (de)insertion process are underway, as are investigations to probe the kinetics of ion transport. Although the material is far from optimized at present, we anticipate significant improvement by using advanced coatings to increase surface conductivity, and by tuning crystallite size/morphology.

In summary, these findings for the two-dimensional electrode material A_2FePO_4F redefine the scope for new polyanion framework materials. The most important aspect is the ability to use a sodium iron phosphate directly as a cathode in a Li-ion cell. This offers significant advantages with respect to cost and lithium availability, and the possibility of developing viable Na-ion cells. In addition, this new iron phosphate exhibits two-dimensional ion conduction paths, coupled with unusual solid-solution-like electrochemical behaviour that can be correlated with structural properties: namely isostructural end members/intermediates and a low-strain volume change on redox. This is in contrast to the two-phase behaviour exhibited by most other members of the phosphate family. These guidelines provide scope for further investigation that will lead to a broader understanding of developing solid-solution regimes in localized small-polaron conductors. Finally, both the nature of the cation and anion clearly alter structure and hence ion transport pathways. Sodium- and lithium-ion metal (fluoro)phosphates prepared at high temperature are rarely isostructural, and hence this offers exciting possibilities for the development of new compositions and architectures.

METHODS

SINGLE-CRYSTAL DIFFRACTION ANALYSIS OF Na_2FePO_4F

A 0.150 × 0.096 × 0.030 mm pale green crystal grown in a Na_2PO_3F flux was mounted on a nylon fibre with perfluoropolyether oil. Data were collected at 295 K using a Bruker APEX CCD (charge-coupled device) platform diffractometer with monochromated Mo Kα ($\lambda = 0.7107$ Å) radiation. Data collection and reduction were carried out with the Bruker AXS SAINT and SMART5.0 programs respectively; the parameters are listed in the Supplementary Information. The final unit-cell parameters were determined from 6,924 reflections. A total of 1,839 independent reflections were used for the solution by least-square structural refinement (F^2) using the Bruker SHELXTL package. The final R, $wR(F^2)$ and goodness of fit were $R = 2.94\%$, 6.60% and 1.417 respectively. Full crystallographic details will be published elsewhere.

© 2007 Nature Publishing Group

SYNTHESIS OF Na_2FePO_4F

For sol–gel synthesis, stoichiometric amounts of $Fe(CH_3COO)_2$ (Alfa Aesar), $NaCH_3COO$ (BDH, 99%), NaF (Aldrich, 99%) and H_3PO_4 were stirred in a solution of dimethoxyethane and the solvent was then evaporated. The homogeneous gel was fired at 300 °C under flowing Ar for 2 h. The powder was subjected to further heating at 525–625 °C for 6 h. Solid-state synthesis of a pure single phase was accomplished using stoichiometric amounts of $Fe(C_2O_4)\cdot 2H_2O$ (Aldrich, 99%), $NaHCO_3$ (BDH, 99.7%), NaF (Aldrich, 99%) and $NH_4H_2PO_4$ (BDH, 99%) which were ball-milled in silicon nitride media for 6 h. The powder was fired at 300 °C under flowing Ar for 2 h. The powder was further sintered at 525–625 °C for 6 h. The carbon content was determined from gravimetric analysis after dissolution of the inorganic phase.

SYNTHESIS OF Na_xFePO_4F, $x < 2$

Powder samples of pure Na_2FePO_4F were oxidized with stoichiometric amounts of $NOBF_4$ in acetonitrile for 15 h to obtain the desired sodium content.

SYNTHESIS OF $(Li_xNa_{2-x})FePO_4F$

Ion exchange of Na_2FePO_4F was carried out in a refluxing solution of 1 M LiBr in acetonitrile for 6–18 h to obtain $(Li_xNa_{2-x})FePO_4F$ with various Li/Na ratios. The material $LiNaFePO_4F$ (Li/Na ratio of 1:1) was obtained by reducing $NaFePO_4F$ with LiI in acetonitrile for 6 h.

MATERIALS CHARACTERIZATION

Powder XRD of all materials was carried out on a Bruker D8-Advantage powder diffractometer using Cu-Kα radiation ($\lambda = 1.5405$ Å) from $2\theta = 10$ to 80° at 1 s per step of 0.02°. X-ray data sets were refined by conventional Rietveld methods using the GSAS package with the EXPGUI interface[26]. The background, scale factor, zero point, lattice parameters, atomic positions and coefficients for the peak shape function were iteratively refined until convergence was achieved. SEM samples were coated with gold and examined in a LEO 1530 field-emission SEM equipped with an EDX attachment. Images were recorded at 10 kV with a secondary electron detector. TEM imaging and EDX spot elemental analysis were carried out on powders supported on a 200 mesh Cu grid using a Hitachi S5200 operating at 30 kV in scanning TEM mode.

ELECTROCHEMISTRY

Samples of electrochemically active materials were mixed with carbon black and polyvinylidene fluoride in a 75:15:10 weight ratio. The electrochemical performance was evaluated using 2,220 coin cells, using a lithium metal anode and 1 M $LiPF_6$ in ethylene carbonate/dimethyl carbonate solution. Room-temperature galvanostatic cycling was carried out between 2.0 and 4.5 V with a current density of 0.068 mA cm^{-2} corresponding to a C/10 rate.

Received 16 January 2007; accepted 1 June 2007; published 9 September 2007.

References

1. Bruce, P., Scrosati, B., Tarascon, J.-M. & van Schalkwijk, W. Nanostructured materials for advanced energy conversion and storage devices. *Nature Mater.* **4**, 366–377 (2005).
2. Herle, P. S., Ellis, B. & Nazar, L. F. Nanonetwork conduction in olivine phosphates. *Nature Mater.* **3**, 147–152 (2004).
3. Padhi, A. K., Nanjundaswamy, K. S. & Goodenough, J. B. Phospho-olivines as positive electrode materials for rechargeable lithium batteries. *J. Electrochem. Soc.* **144**, 1188–1194 (1997).
4. Maxisch, T., Zhou, F. & Ceder, G. *Ab initio* study of the migration of small polarons in olivine Li_xFePO_4 and their association with lithium ions and vacancies. *Phys. Rev. B* **73**, 104301 (2006).
5. Delacourt, C., Poizot, P., Tarascon, J. M. & Masquelier, C. The existence of a temperature-driven solid solution in Li_xFePO_4. *Nature Mater.* **4**, 254–260 (2005).
6. Yamada, A. *et al.* Room temperature miscibility gap in Li_xFePO_4. *Nature Mater.* **5**, 357–360 (2006).
7. Ellis, B., Perry, L. K., Ryan, D. H. & Nazar, L. F. Small polaron hopping in Li_xFePO_4 solid solutions: Coupled lithium-ion and electron mobility. *J. Am. Chem. Soc.* **128**, 11416–11422 (2006).
8. Delacourt, C., Poizot, P., Levasseur, S. & Masquelier, C. Size effects on carbon-free $LiFePO_4$ powders: The key to superior energy density. *Electrochem. Solid-State Lett.* **9**, A352–A355 (2006).
9. Meethong, N., Huang, H.-Y., Carter, W. C. & Chiang, Y.-M. Size-dependent lithium miscibility gap in nanoscale $Li_{1-x}FePO_4$. *Electrochem. Solid-State Lett.* **10**, A134–A138 (2007).
10. Yin, S. C., Edwards, R., Taylor, N., Herle, P. S. & Nazar, L. F. Dimensional reduction: Synthesis and structure of layered $Li_3M(PO_4)_2F_2$ (M = V, Cr). *Chem. Mater.* **18**, 1745–1752 (2006).
11. Dutreilh, M., Chevalier, C., El-Ghozzi, C. M. & Avignant, D. Synthesis and crystal structure of a new lithium nickel fluorophosphate $Li_2[NiF(PO_4)]$ with an ordered mixed anionic framework. *J. Solid State Chem.* **142**, 1–5 (1999).
12. Okada, S., Ueno, M., Uebou, Y. & Yamaki, J. Electrochemical properties of a new lithium cobalt fluorophosphate $Li_2[CoF(PO_4)]$. Abstract # 301, *IMLB-12* (2004).
13. Barker, J., Saidi, M. Y. & Swoyer, J. L. Electrochemical insertion properties of the novel lithium vanadium fluorophosphate, $LiVPO_4F$. *Electrochem. Solid-State Lett.* **6**, A1–A4 (2003).
14. Barker, J., Gover, R. K. B., Burns, P. & Bryan, A. J. Hybrid-ion. A lithium-ion cell based on a sodium insertion material. *Electrochem. Solid-State Lett.* **9**, A190–A192 (2006).
15. Coetzer, J. A new high energy density battery system. *J. Power Sources* **18**, 377–380 (1986).
16. Stevens, D. A. & Dahn, J. R. High capacity anode materials for rechargeable sodium-ion batteries. *J. Electrochem. Soc.* **147**, 1271–1273 (2000).
17. Stevens, D. A. & Dahn, J. R. The mechanisms of lithium and sodium insertion in carbon materials. *J. Electrochem. Soc.* **148**, A803–A811 (2001).
18. Kabalov, Y. K., Simonov, M. A. & Belov, N. V. Crystal structure of basic iron phosphate ($Na_2Fe[PO_4]OH$). *Dokl. Akad. Nauk SSSR* **215**, 850–853 (1974).
19. Sanz, F., Parada, C. & Ruiz-Valero, C. Crystal growth, crystal structure and magnetic properties of disodium cobalt fluorophosphate. *J. Mater. Chem.* **11**, 208–211 (2001).
20. Yakubovich, O. V., Karimova, O. V. & Mel'nikov, O. K. The mixed anionic framework in the structure $Na_2MnF(PO_4)$. *Acta Crystallogr. C* **53**, 395–397 (1997).
21. Rastsvetaeva, R. K., Maksimov, B. A. & Timofeeva, V. A. Crystal structure of a new Na,Fe-phosphate $Na_5Fe(PO_4)_2F_2$. *Dokl. Akad. Nauk DAKNE* **350**, 499–502 (1996).
22. Le Meins, J.-M., Crosnier-Lopez, M. P., Hemon-Ribaud, A. & Courbion, G. Phase transitions in the $Na_3M_2(PO_4)_2F_3$ family: Synthesis, thermal, structural, and magnetic studies. *J. Solid State Chem.* **148**, 260–277 (1999).
23. Doeff, M. M., Wilcox, J. D., Kostecki, R. & Lau, G. Optimization of carbon coatings on $LiFePO_4$. *J. Power Sources* **163**, 180–184 (2006).
24. Yin, S. C., Grondey, H., Strobel, P. & Nazar, L. F. Electrochemical structure-property relationships in $Li_{3-x}V_2(PO_4)_3$. *J. Am. Chem. Soc.* **125**, 326–327 (2003).
25. Masquelier, C., Padhi, A. K., Nanjundaswamy, K. S. & Goodenough, J. B. New cathode materials for rechargeable lithium batteries: The 3-D framework structures $Li_3Fe_2(XO_4)_3$ (X = P, As). *J. Solid State Chem.* **135**, 228–234 (1998).
26. Toby, B. H. EXPGUI, a graphical user interface for GSAS. *J. Appl. Crystallogr.* **34**, 210–213 (2001).

Acknowledgements

L.F.N. gratefully acknowledges the financial support of NSERC through its Discovery and Strategic programs.
Correspondence and requests for materials should be addressed to L.F.N.
Supplementary Information accompanies this paper on www.nature.com/naturematerials.

Competing financial interests

The authors declare no competing financial interests.

Reprints and permission information is available online at http://npg.nature.com/reprintsandpermissions/

© 2007 Nature Publishing Group

View publication stats